



Microstructural changes due to heat-treatment of annealing and their effect on the creep behavior of self-reinforced silicon nitride ceramics

Q. Wei ^{a,*}, J. Sankar ^a, J. Narayan ^b

^a NSF Center for Advanced Materials and Smart Structures, Department of Mechanical Engineering, NC A&T State University, McNair Hall, West Market Street, Greensboro, NC 27411, USA

^b Department of Materials Science and Engineering, North Carolina State University, Raleigh, NC 27695-7916, USA

Received 30 May 2000; received in revised form 31 July 2000

Abstract

In order to understand the improvement of creep resistance by furnace and microwave annealing, we have investigated the effect of heat-treatment on the microstructural characteristics of the crept self-reinforced silicon nitride (Si_3N_4) ceramic GS44. X-ray diffraction was performed on the as-sintered and heat-treated samples to study the phase changes due to annealing treatment. Optical microscopy and scanning electron microscopy (SEM) were used to study the fracture surface and to identify the creep mechanism. High resolution and analytical transmission electron microscopy (TEM) were employed to analyze the microstructures of the crept samples with as-received and heat-treated conditions. It has been reported that both conventional furnace and microwave annealing enhance the creep resistance of the material, and microwave annealing had the most significant effect. Fractography showed that the microwave annealed samples exhibits least creep damage. Furnace annealing also reduces the creep damage, but the effect is far less as compared to microwave annealing. Scanning electron microscopy (SEM) analysis showed significant amount of multiple-junction cavitation in the creep-tested samples. TEM observations showed significant devitrification of the amorphous phases in the microwave annealed specimens, as verified by micro-diffraction studies of the junction phases. This is also confirmed by X-ray diffraction and high-resolution lattice image of the triple junction phases. The microstructural observations were combined with a recent model of the effect of amorphous residues in ceramics on the creep behavior to explain the improvement in the creep resistance due to annealing. © 2001 Elsevier Science B.V. All rights reserved.

Keywords: Silicon nitride; Ceramics; Microwave annealing; Microstructures; Creep

1. Introduction

Because of its unique properties, silicon nitride (Si_3N_4) is one of the most promising candidates for advanced engine parts among the non-oxide ceramics. For example, silicon nitride has very high strength, very low thermal expansion coefficient (which leads to excellent thermal shock resistance), and chemical stability at high temperatures. However, like most ceramics, conventional equi-axed Si_3N_4 ceramics suffer from poor fracture toughness that leads to low damage tolerance and poor reliability (small Weibull modulus). For the

past two decades, enormous effort has been exercised to improve the fracture toughness of ceramics by means of reinforcement [1], phase transformation toughening [2], microstructure designing [3], etc. In mid 80s, Si_3N_4 ceramics with high fracture toughness had been produced through composition and microstructure design such that the fracture toughness reached $\sim 10 \text{ MPa}\cdot\text{m}^{1/2}$ [4]. One of the newer Si_3N_4 ceramics, GS44, has been developed by AlliedSignal with yttria, alumina and magnesia as sintering aids. This material has moderate to high fracture toughness ($> 8.0 \text{ MPa}\cdot\text{m}^{1/2}$) and quite high room-temperature strength. The elongated grains work in such a way that crack bridging, pull-out of these grains and crack deflection mechanisms effect the reinforcement and lead to much improved fracture toughness [5]. However, it was found that the creep

* Corresponding author. Tel.: +1-336-3347411, ext.: 2107; fax: +1-336-3347417.

E-mail address: quiming@ncat.edu (Q. Wei).

resistance of this material is remarkably decreased at temperatures $> 1100^{\circ}\text{C}$ [6].

It is well recognized that the amorphous grain boundary and multiple junction phases in silicon nitride ceramics lead to creep processes via solution-precipitation, grain boundary sliding and cavitation at high temperatures [7–12]. It was suggested [8] that the amorphous phase can influence the creep behavior of a ceramic in three ways. First, it may act as a rapid diffusion path whereby material from the crystalline phase is dissolved into the amorphous phase in regions under compression, diffuses through it, and then re-deposits in regions under tension (solution-re-precipitation mechanism). Secondly, the amorphous phase can be redistributed from regions under compression to those under tension by viscous flow. Finally, the multiple junctions provide preferential sites for cavitation, which provides an additional, even dominant creep mechanism for silicon nitride ceramics. A recent theoretical consideration [13] on the tensile creep of silicon nitride has even correlated the creep strain rate with the amount of amorphous second phase, which showed that the creep strain rate increases dramatically with the fraction of the amorphous second phase. According to the model, it is desirable to minimize the amount of amorphous second phases, or to re-crystallize these phases by any means possible.

Liu et al. [14] at Oak Ridge National Laboratory have studied the effect of heat-treatment on the creep behavior of GS44. They conducted conventional furnace annealing and microwave annealing on the materials and carried out tensile creep tests on specimens machined out of the as-received and heat-treated ceramic tiles. Improvement in creep behavior by microwave annealing has been reported. However, they did not provide microstructural analysis and fractography of the various samples. In order to understand the high temperature creep resistance of this material upon heat-treatment, we studied microstructural changes on the samples after conventional furnace and microwave annealing. Therefore, this work is a follow-up of the work by Liu et al. [14]. Tensile creep tests were conducted by Liu et al. [14] on as-sintered, furnace and microwave annealed GS44 samples. The creep-tested samples were then analyzed in this work for fractography and microstructural changes. This is one of the few reports on the microstructural changes associated with microwave annealing of silicon nitride ceramics. It should be noted that microwave heating has been explored for the sintering of silicon nitride ceramics, which as proposed by some investigators, is superior to conventional sintering process in terms of end-product performance and cost [15–18].

2. Experimental details

For comparison, the creep behavior of the as-sintered GS44 was first studied in our laboratory under the same conditions as reported in Ref. [14]. In order to acquire more detailed information of the creep properties of this material, we also performed creep tests at varied temperatures and under different loads.

All the heat-treatments and the creep tests were conducted by K.C. Liu et al. at Oak Ridge National Laboratories [14]. All the microstructural changes and fractographic details were observed at the NSF Center for Advanced Materials and Smart Structures (NSF-CAMSS), North Carolina A&T State University. The microwave processing is briefly summarized as follows. Each tile was microwave annealed at 1400, 1500 and 1600 $^{\circ}\text{C}$ for 20 h in search of the optimum annealing temperature. Two of the as-furnished tiles were annealed initially at 1100 $^{\circ}\text{C}$ for 10 h followed by final annealing at 1200 $^{\circ}\text{C}$ for 10 h. The tile was sandwiched between two plates of boron dioxide to facilitate heat conduction in order to anneal the tile as evenly as possible and to avoid severe localized heating. To evaluate the effectiveness of microwave annealing compared to conventional annealing, a tile was aged at 1200 $^{\circ}\text{C}$ in air for 10 h in a conventional furnace. Creep tests were performed on standard button-head samples in lever-arm creep machines equipped with a low profile, two-zone controlled, resistance-heating furnace. Creep strain was measured with a mechanical extensometer. Microwave annealed specimens were designated with a prefix of ‘MA’ followed by the first and second digits of its annealing temperature with specimen number trailing a hyphen, as ‘MA12-4’ symbolizing microwave annealed at 1200 $^{\circ}\text{C}$, specimen No. 4; likewise with ‘FA’ and ‘AS’ symbolizing furnace annealing and as-sintered conditions. For further detailed information regarding heat-treatments and creep testing please refer to Liu et al. [14].

The fracture surface of the specimens was investigated using both optical microscope (for low magnification, damage type recognition) and scanning electron microscope (SEM). Samples for transmission electron microscopic observations were cut from the as-sintered and creep tested specimens close to the fracture surface. The samples were polished to 50–80 μm and then a crater was made using a dimple grinder, with the center of the crater only about 10 μm or less. The samples were then ion milled to electron transparency. High-resolution TEM observations were performed on TOPCON-002B with 1.8 \AA point-to-point resolution at the first Scherzer focus. We also performed analytical TEM observations on the samples to study the triple-junction phases, especially their changes upon heat-treatment.

3. Results and discussion

This section will be divided into three parts. First, creep results obtained in this laboratory and those obtained by Liu et al. [14] will be described and briefly discussed. The discussion will focus on the comparison among the specimens under different initial conditions before creep. This will be followed by fractography of the creep-tested specimens to identify the fracture surface features and to establish possible creep mechanisms involved. The final part will be focused on X-ray diffraction and transmission electron microscopy of the as-sintered and heat-treated specimens to understand the microstructural changes associated with annealing treatments, and provide basis for the understanding of the effect of heat-treatments on the creep properties of this self-reinforced silicon nitride ceramic.

3.1. Tensile creep tests

Fig. 1 gives the creep curves obtained for as-sintered GS44 in our laboratory. There are three creep curves; each one of them was obtained at the same temperature of 1200°C, but under different stress levels. The stress exponent at this temperature is close to 2.0. The curve obtained under 100 MPa exhibits three distinct regimes, i.e. primary, secondary (steady-state) and tertiary creep. Detailed TEM observations of these and other creep-tested specimens from this laboratory have been reported elsewhere [19,20].

All specimens from Liu et al. [14] were creep tested at 1200°C mostly under constant loads until rupture occurred. A few microwave-annealed specimens were tested with a step-up load history in order to complete the tests in a reasonable time period. Detailed information regarding the creep test results is referred to Ref. [14]. Fig. 2 (a) is a comparison of creep curves for specimens tested in the as-sintered (or unannealed), furnace annealed, and various microwave annealed conditions. The base loading stress was 100 MPa. It should be pointed out that only five specimens could be

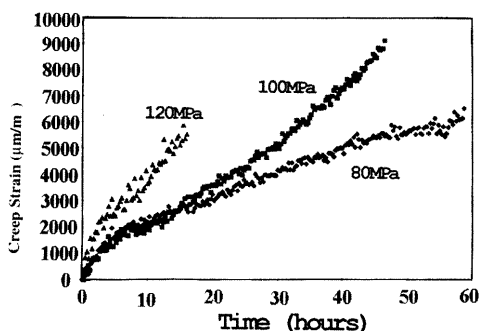


Fig. 1. Creep curves obtained for as-sintered GS44 at 1200°C under various stress levels of 80, 100 and 120 MPa.

machined out of each tile. Therefore, MA12-5 is from a different tile than MA12-7, -9, and -10 which are from the same tile. There exists some inconsistency in the efficiency of microwave annealing. This is observed through the creep curves of MA12-7, -9, and -10 that showed that microwave annealing did not result in any detectable improvement in the creep resistance of the material. Liu et al. [14] postulated that this inconsistency is due to material variations and test machine bias on creep properties. Fig. 2 (a) shows that higher temperature annealing does not improve creep resistance, but in most cases resulted in some loss of creep resistance as compared to the as-sintered specimens (see creep curves of MA14-3, MA15-6 and MA16-11). Fig. 2 (b) is a comparison of creep curves for specimens tested in the as-sintered, furnace annealed and microwave annealed conditions with a base stress of 120 MPa. Notice that all the annealing treatments for these specimens were performed exclusively at 1200°C. The improvement of creep behavior of the annealed samples can be clearly established. The creep curve of microwave annealed sample, MA12-2 was obtained through the step-up test mode in order to complete the creep test in a reasonable time. Fig. 2 (c) shows the creep curves of four specimens that have been microwave annealed at 1200°C. The general tendency of improved creep resistance by microwave annealing can be observed, though some discrepancy in the same tile is observed (see creep curve MA12-4 that exhibits relatively low creep resistance than the rest of the samples, however much more creep resistant than the as-sintered specimens). The discrepancy was attributed to the variation of specimen positions in the same tile, which may result in non-uniform temperature distribution during microwave annealing.

Therefore, from overall observations of creep curves, it can be seen that microwave annealing at 1200°C enhances the creep resistance of GS44. Furnace annealing also improves the creep resistance of GS44, but the effect is far less compared to microwave annealing. Still, some inconsistency has been observed in the creep test results. Though a complete understanding should be based on more experimental observations, the work of Liu et al. [14] could serve as a good starting point for further investigation.

3.2. Fractography of the creep-tested specimens

To study the fractographic features of creep tested samples under different conditions, the fracture surfaces of the specimens were first observed by optical microscope at low magnification. Fig. 3 is a series of fracture surfaces of various specimens. The areas indicated by the arrows are features due to creep damage [21]. Other features that appear in those fracture surfaces include mist, mirror and hackle regions. The creep damage

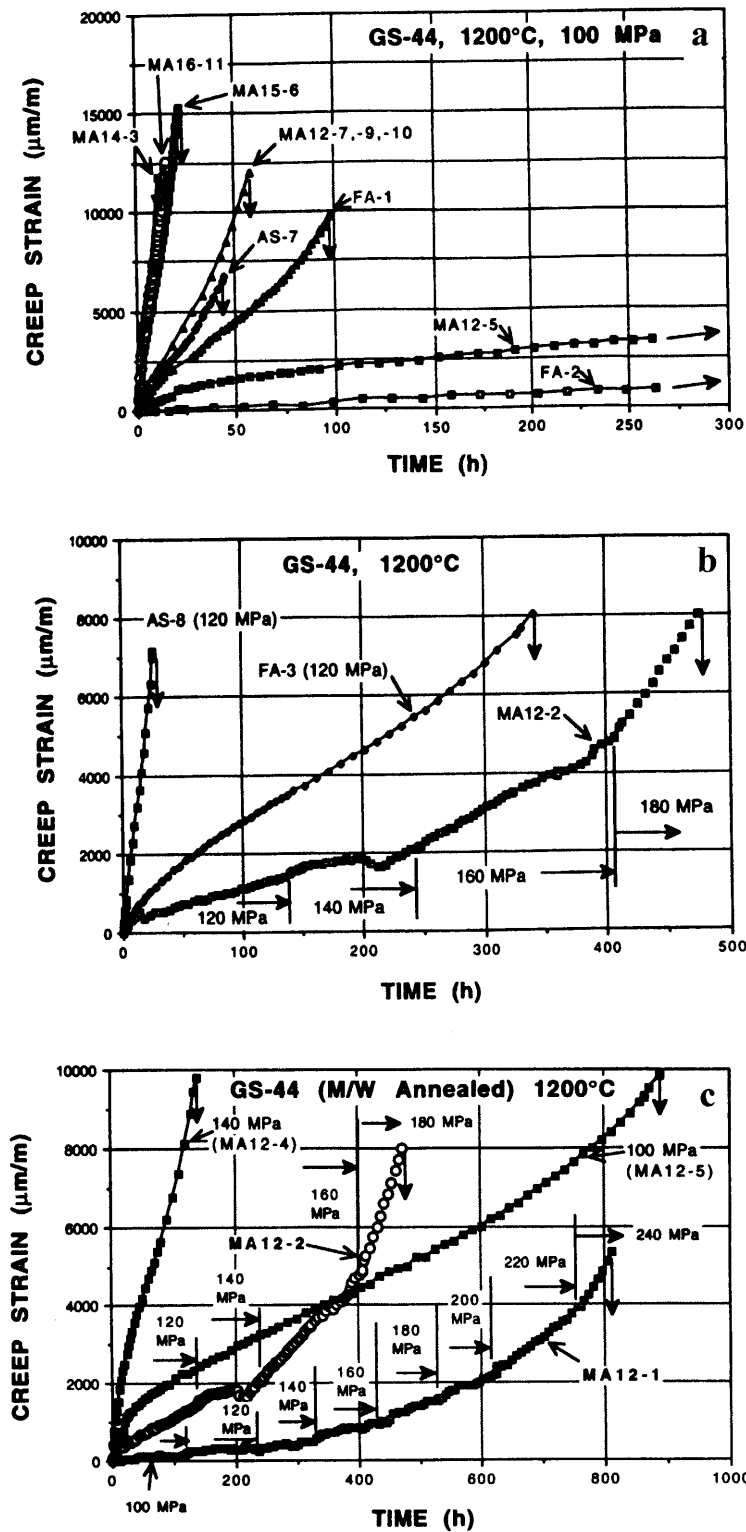


Fig. 2. (a) Creep curves of different specimens of GS44 under a stress level of 100 MPa. The enhancement of creep resistance by microwave annealing at 1200°C is demonstrated. See the text for the details of these curves. (b) Creep curves of GS44 as-sintered, furnace annealed and microwave annealed at 1200°C. Base stress for these curves is 120 MPa. (c) Creep curves of GS44 after microwave annealing at 1200°C. The curves show significant improvement in creep resistance except for specimen MA12-4, which is still much more creep resistant than the as-sintered material [14].

zone is usually rough and its formation can be attributed to the damage zone evolution, which involves

extensive microcracking resulting from the linkage of cavities [22]. Fig. 3 (a) shows the creep fracture surface

of as-sintered GS44. The creep test was conducted at a base load of 120 MPa and 1200°C. The creep life is about 25 h, which is similar to the results collected in our laboratory. A significant amount of creep damage zone (rough surface) can be observed in the fracture surface of the as-sintered GS44. The rest of the fracture surface consists of relative smooth features, resulting from rapid crack growth [22]. Extensive SEM and TEM observations did not reveal any lenticular cavities along the grain boundaries; all the cavities were found to be formed on the multiple junction pockets [6,19]. Fig. 3 (b) is the creep fracture surface of a furnace-annealed sample. It is observed that the creep damage area in this specimen is relatively small as compared to the as-sintered specimen. Again, the rest of the fracture surface consists of smooth areas, resulting from fast fracture, in addition to other features such as mist, mirror and hackle region. However, the size of the hackle region is significantly increased in this specimen. Fig. 3 (c) is the creep fracture surface of a microwave-annealed specimen (MA12-5). It exhibits significantly reduced creep damage area, and consists of a large hackle region and a relatively small mirror region. This again shows that microwave annealing at an appropriate temperature can remarkably enhance the creep resistance of GS44.

Detailed fractographic features were analyzed using SEM under higher magnifications. Fig. 4 (a) shows an SEM image of the creep fracture surface of as-sintered GS44. The specimen is the same as that of Fig. 3(a). A large-sized flaw can be seen from this micrograph, which is close to the surface of the creep specimen. The flaw might be due to an impurity inclusion. Our previous studies on the creep behavior of as-sintered GS44 demonstrated that the creep mechanisms are dominated by grain boundary sliding and cavitation process [6]. Fig. 4 (b) shows a large amount of cavities, all located at the multiple junction pockets. The specimen is absent from lenticular cavities, in agreement with our previous report on the as-sintered GS44 [6]. Fig. 4 (c) is an SEM micrograph of the creep fracture surface of a GS44 specimen that was microwave annealed at 1200°C. The amount of cavities in this specimen is similar to that of the as-sintered GS44. Fig. 4 (d) is an SEM micrograph of the creep fracture surface of GS44 that was furnace-annealed at 1200°C. The features in this specimen are somewhere between those of as-sintered and microwave annealed specimens.

The creep resistance of a material could be reflected by the creep strain rate and the creep rupture life. The creep strain rate is usually taken from the secondary creep regime, namely the steady-state creep regime. The

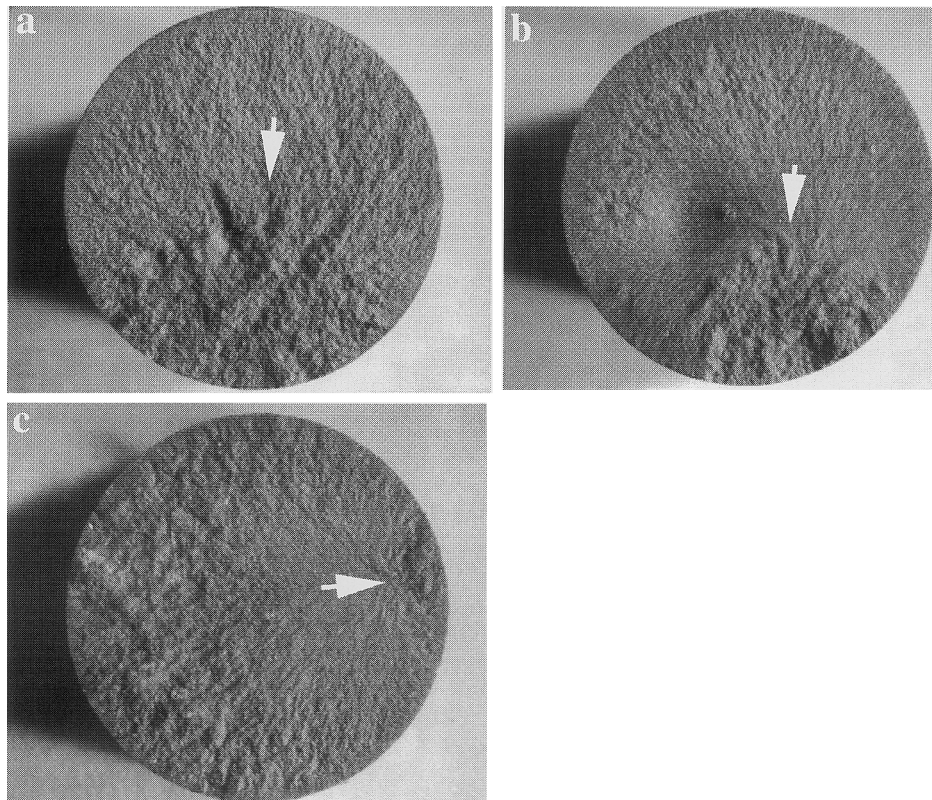


Fig. 3. Optical micrograph of the creep fracture surfaces of GS44 silicon nitride ceramics tested at 1200°C. (a) As sintered; (b) furnace annealed and (c) microwave annealed at 1200°C. The creep damage zone in all the samples are indicated by arrows. The images clearly show that the size of creep damage zone in the microwave-annealed specimen is significantly reduced as compared with the as-sintered specimen.

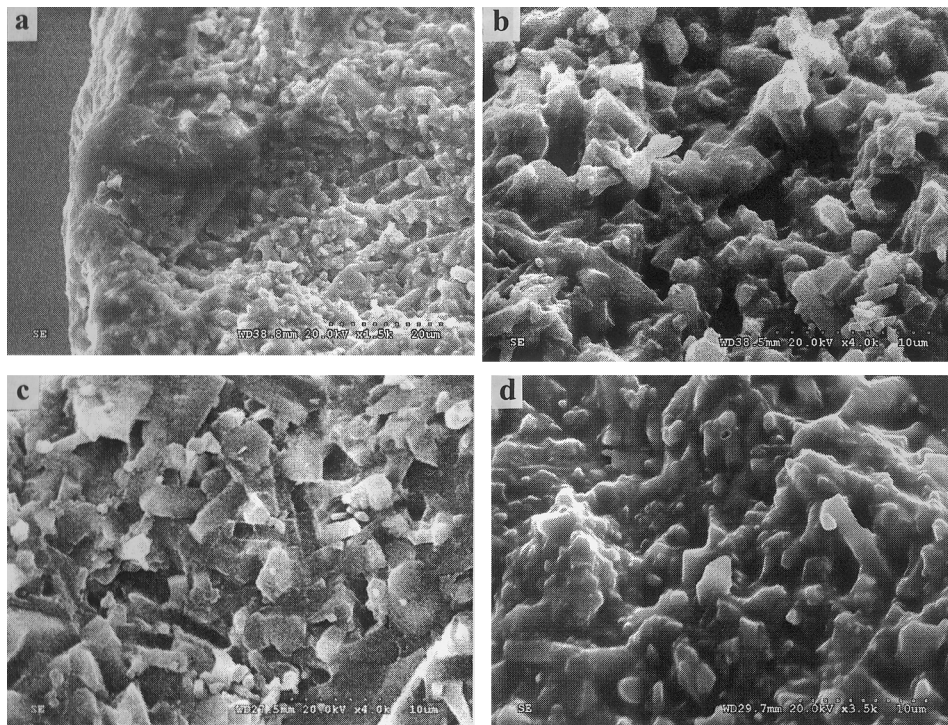


Fig. 4. SEM images of the creep fracture surfaces of the as-sintered GS44 Si_3N_4 showing a large-sized flaw (a) and a large population of cavities (b). SEM micrographs of GS44 creep fracture surface of the tested specimens microwave-annealed at 1200°C (c) and furnace-annealed (d).

smaller the creep strain rate, the higher the creep resistance of the material. It is interesting to notice in the creep curves given in Fig. 1 and Fig. 2 that while there exists remarkable difference in the creep resistance of the as-sintered and annealed specimens, the total creep strain did not exhibit significant difference. It is reported that cavitation contributes substantially to tensile creep in silicon nitride ceramics [10–13]. It has even been considered by some investigators [12] that cavitation of the interstitial silicate phase accompanies creep under all conditions, and accounts for nearly all of the measured strain. Our observations are in accordance with these proposed creep mechanisms. However, the creep resistance improvement in the heat-treated specimens needs further consideration. Detailed microstructural changes associated with heat-treatment might help reveal the underlying explanations for the enhancement of creep resistance by microwave annealing.

3.3. X-ray diffraction and TEM studies of the as-sintered and annealed specimens

In order to understand the fine scale microstructural changes associated with annealing and to compare the microstructures between the as-sintered and annealed specimens, we performed X-ray diffraction experiments and detailed transmission electron microscopy (TEM) studies on certain specimens. The purpose of X-ray diffraction is to investigate the possible phase changes

accompanying heat-treatment. TEM observations were focused on the changes of the amorphous residue from the sintering additives associated with annealing.

The complete information on the chemical composition of GS44 is proprietary to AlliedSignal and is not available to the public. However, energy dispersive spectroscopy of the specimens indicated that the sintering aids consist of a combination of yttria, magnesia and alumina. Fig. 5 is the X-ray diffraction result of the as-sintered GS44. It consists of X-ray diffraction peaks

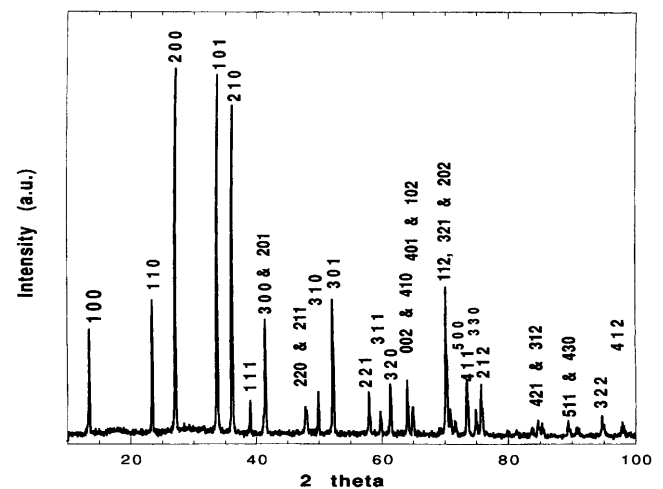


Fig. 5. X-ray diffraction of as-sintered GS44 showing peaks from $\beta\text{-Si}_3\text{N}_4$ only.

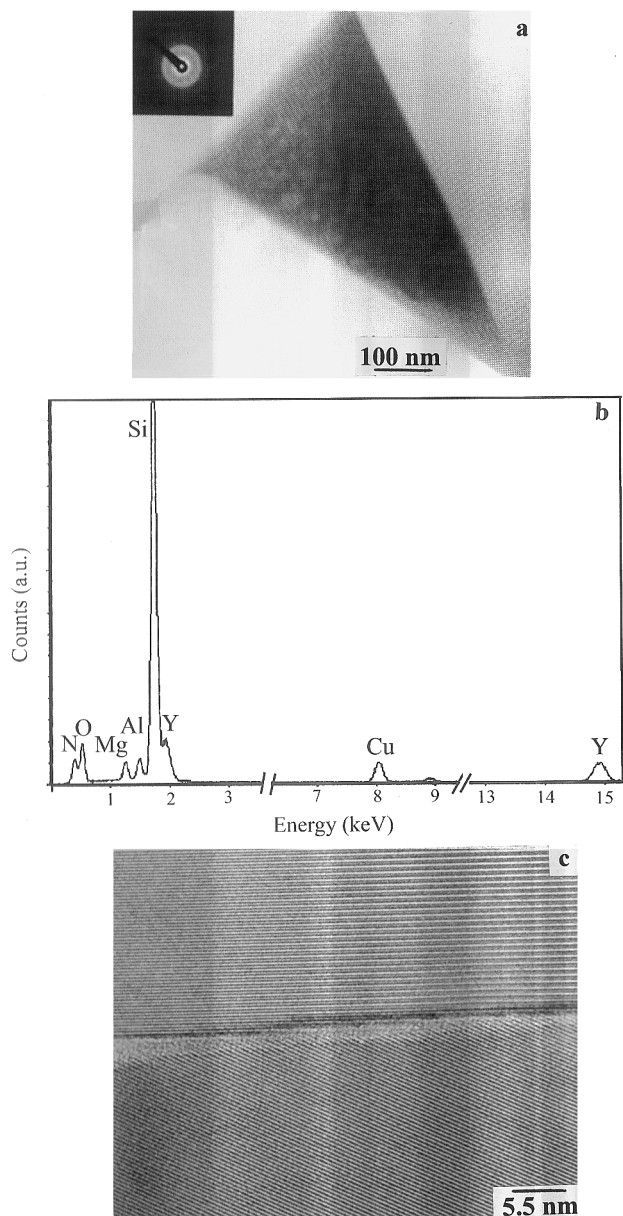


Fig. 6. Bright field TEM image of a triple junction phase in as-sintered GS44 and selected area diffraction pattern showing the amorphous state of the triple junction phase (a); EDX analysis of the triple junction shows that it consists of yttria, alumina and magnesia, in addition to silica (b); high-resolution TEM lattice image of the grain boundary phase of about 3.0 nm in thickness separating two Si_3N_4 grains (c).

exclusively from the $\beta\text{-Si}_3\text{N}_4$ phase. No peaks from $\alpha\text{-Si}_3\text{N}_4$ or from other phases than Si_3N_4 are detected. Fig. 6 (a) is a TEM micrograph of the as-sintered GS44 showing a typical triple junction phase. The inset in Fig. 6 (a) is a selected area diffraction (SAD) pattern from the triple junction phase. This SAD pattern exhibits diffuse rings only, indicating fully amorphous state of the triple junction phase. In order to obtain composition information of the triple junction phase, energy dispersive X-ray (EDX) spectroscopy was per-

formed on the triple junction phase, with the result given in Fig. 6 (b). We refrained from quantitative analysis of chemical composition of the triple junction phase due to the difficulty in acquiring precise data for oxygen and nitrogen.

Apart from multiple junction amorphous phases, there are still grain boundary phases with varied thickness, from the 'equilibrium thickness' [23] of about 1.0 ~ 1.5–3.0 ~ 5.0 nm. Fig. 6 (c) shows a high resolution TEM lattice image of two Si_3N_4 grains separated by the amorphous grain boundary phase of ~ 3.0 nm in thickness.

Detailed TEM observations on the creep-tested as-sintered GS44 specimens have been reported elsewhere [19]. Briefly, a large amount of strain whorls, large dislocation densities in certain silicon nitride grains, multiple junction cavities, grain boundary sliding, and so on, were observed in the creep-tested as-sintered GS44 specimens. It was concluded that for the as-sintered GS44, the dominant creep deformation mechanism is cavitation assisted by grain boundary sliding, which might also be assisted by dislocation generation at the contact locations between two silicon nitride grains. Fig. 7 (a) is a bright field TEM micrograph of a creep-tested GS44 which was microwave annealed at 1200°C, showing cavities and strain whorls. Fig. 7 (b) shows heavy plastic deformation through dislocation process in certain silicon nitride grains. Again, as argued in our previous work [19], since the occurrence of dislocations is localized, it can not account for the creep strain of the whole specimen. Therefore, the overall microstructure of the creep-tested specimens did not show much difference with and without annealing. However, more detailed analysis on the triple junction phases given below shows significant changes in the annealed specimens. Fig. 8 (a) is a bright field TEM image of a microwave annealed (1200°C) GS44 sample showing silicon nitride grains and triple junction phases, with the triple junction phases indicated by arrows. Fig. 8 (b) is a micro-diffraction (μ -diffraction) pattern taken from the triple junction phase. It can be clearly seen that this pattern shows spots, which is typical of crystalline structure. The small tilt range of the goniometer of our TEM prohibits us from obtaining an in-zone diffraction pattern of this phase. However, the crystallinity can be clearly established from the spot pattern. In other words, the triple junction phase in Fig. 8 (a) has been devitrified during the annealing process. Fig. 8 (c) gives another example of the devitrified triple junction phases, with the micro-diffraction pattern given in Fig. 8 (d).

In order to confirm the TEM observations that annealing treatment devitrified the previously amorphous triple junction phases, we performed X-ray diffraction on the annealed specimen. Fig. 9 (a) is the X-ray diffraction result from a GS44 specimen microwave

annealed at 1200°C (specimen MA12-5). As compared to the as-sintered specimen (Fig. 5), small peaks that are not from β -Si₃N₄ can be observed. These small peaks are located at 2ϕ values of ~ 30 , ~ 57 , ~ 66 , and $\sim 68^\circ$. In order to see these peaks more clearly, we conducted fine scan with smaller step-size and larger count rate around these peaks. Fig. 9 (b) shows such a fine scan from 2ϕ angle 25–35°. A peak at 29 can be observed clearly. Even though we could not establish the crystal structure producing these extra peaks due to

lack of detailed information on the chemical composition of the material, we verify again by X-ray diffraction that crystallization occurred in amorphous sintering aids during annealing treatments.

Fig. 10 (a) is a typical triple junction phase in the microwave annealed GS44 (MA12-5), and Fig. 10 (b) shows the high-resolution lattice image of the silicon nitride grains and part of the triple junction phase. Lattice fringes are visible from the triple junction phase area.

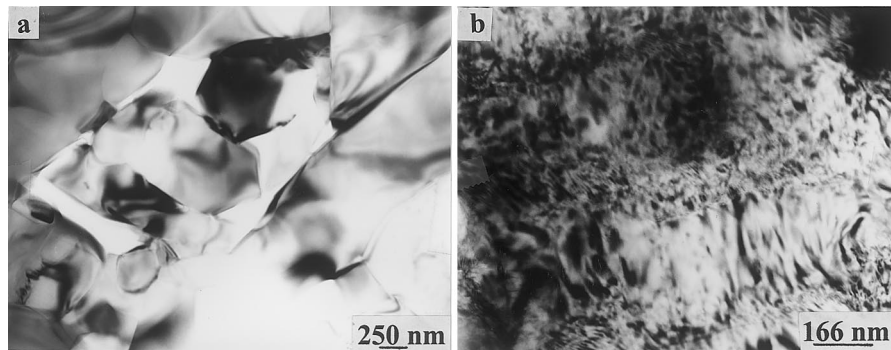


Fig. 7. BF TEM micrograph of a creep-tested GS44, which was microwave annealed at 1200°C, showing cavities and strain whorls (a); and some Si₃N₄ grains have been heavily deformed through dislocation process (b).

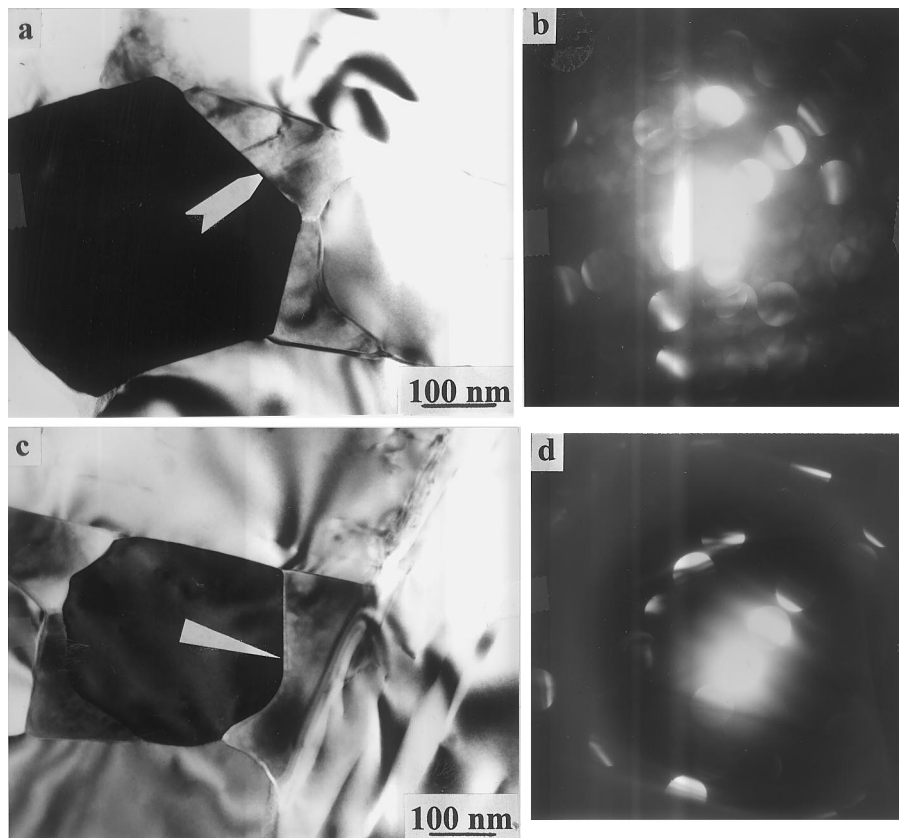


Fig. 8. Bright field TEM micrograph of GS44 microwave annealed at 1200°C, the arrow indicates the triple junction phase (a); microdiffraction from the triple junction phase shows that the triple junction phase has been devitrified (b). In (c) is another TEM image of Si₃N₄ grains and the multiple junction phases indicated by arrows, and μ -diffraction pattern shows that the multiple junction phases have been devitrified (d). Notice no diffuse scattering is visible from the μ -diffraction pattern.

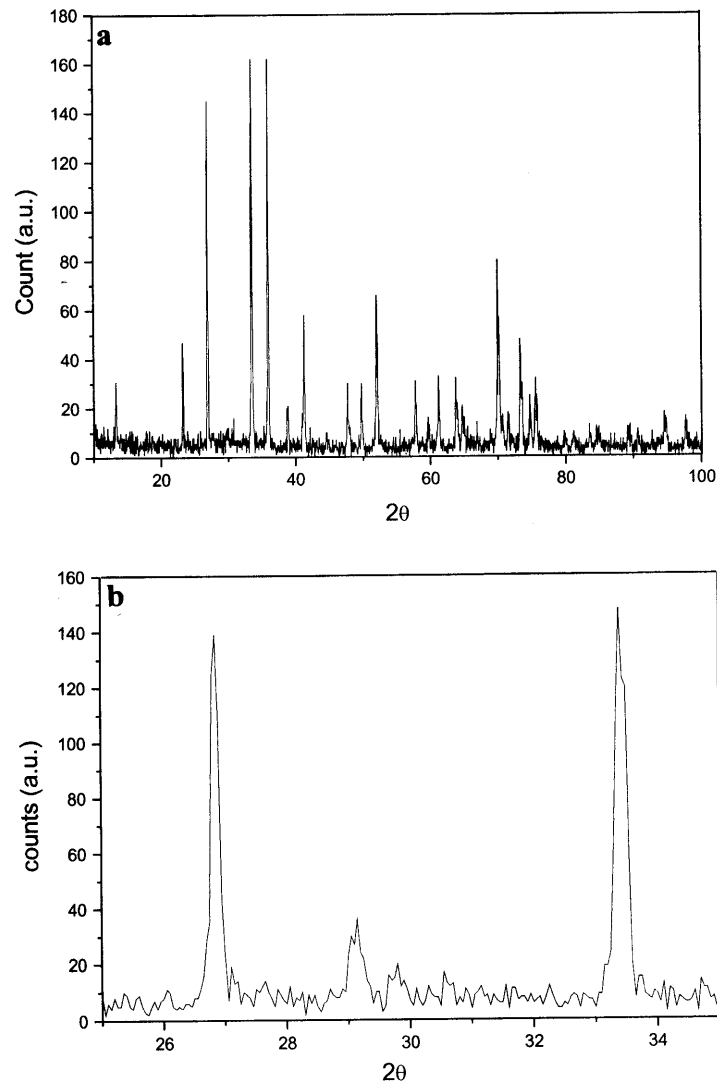


Fig. 9. X-ray diffraction of a GS44 specimen microwave annealed at 1200°C (MA12-5) (a). Compared to Fig. 5, small extra peaks, which can not be attributed to β - Si_3N_4 appear. Fine XRD scan established more clearly the existence of these peaks (b).

As pointed out in the Introduction, amorphous residues in the grain boundaries and multiple junctions in silicon nitride ceramics decreases its creep resistance at high temperature. A review of experimental data by Luecke and Wiederhorn [13] suggests that the rate of formation and growth of cavities in the second phase controls creep in most commercial grades of Si_3N_4 ceramics. They proposed a simple phenomenological model to correlate the creep rate to the applied stress, the Si_3N_4 grain size, the effective viscosity of the deformable phase, and the volume fraction of the deformable phase. The creep strain rate can be expressed as

$$\dot{\varepsilon}_s = A\sigma \exp\left(-\frac{\Delta H}{RT}\right) \frac{\Phi^3}{(1-\Phi)^2} \exp(\alpha\sigma), \quad (1)$$

where A is a constant, σ the applied stress, ΔH the activation energy, R the gas constant, T the absolute

temperature, α some constant, and Φ is the volume fraction of the amorphous phase. From Eq. (1), it is seen that the steady state creep strain rate is proportional to the cube of the volume fraction of the deformation amorphous phase. Therefore, devitrification of the amorphous grain boundary phase or triple junction phase of silicon nitride ceramics explains the enhancement of the creep resistance at high temperature. When the amorphous phases are devitrified through approaches such as heat-treatment, the detrimental effect of these phases on the high temperature creep performance can be alleviated or even eliminated, resulting in much improved creep resistance.

Therefore, the creep test results, X-ray diffraction studies and microstructural observations of the present work demonstrate that microwave annealing can be an efficient route to improve the creep resistance of sintered Si_3N_4 through devitrification of the glass phases.

4. Summary and concluding remarks

We have investigated the effect of heat-treatment on the phase changes and microstructural characteristics of a self-reinforced silicon nitride (Si_3N_4) ceramic GS44 using X-ray diffraction, optical microscopy, scanning electron microscopy and transmission electron microscopy. X-ray diffraction was performed on the as-sintered and heat-treated samples to study the phase changes due to annealing treatment. Optical microscopy and scanning electron microscopy (SEM) were used to study the fracture surface and to identify the creep mechanism. High resolution and analytical transmission electron microscopy (TEM) were employed to analyze the microstructures of the creep samples with as-received and heat-treated conditions. Fractography showed that the microwave annealed samples exhibited the least amount of creep damage. Furnace annealing also reduces the creep damage, but the effect is far less as compared to microwave annealing. Scanning electron microscopy (SEM) analysis showed significant amount of multiple-junction cavit-

tion in the creep-tested samples. TEM observations showed significant devitrification of the amorphous phases in the microwave annealed specimens, as verified by micro-diffraction studies of the junction phases. X-ray diffraction also confirmed the TEM observations. The microstructural changes were combined with a recent model of the effect of amorphous residues in ceramics on the creep behavior to explain the improvement in the creep resistance due to microwave and furnace annealing.

Acknowledgements

The authors would like to thank Dr K.C. Liu from Oak Ridge National Laboratory for supplying the specimens and the creep results. This research was sponsored by DOE, Assistant Secretary for Energy Efficiency and Renewable Energy, Office of Transportation Technologies, as part of the Heavy Vehicle Propulsion System Materials Program under contract DE-AC05-96OR22464 with Lockheed Martin Energy Research Inc. The authors wish to thank Dr Ray Johnson for his continuing support and many helpful technical suggestions through out the program.

References

- [1] P.F. Becher, *J. Am. Ceram. Soc.* 74 (2) (1991) 255–269.
- [2] P.F. Becher, M.V. Swain, M.K. Ferber, *J. Mater. Sci.* 22 (1) (1987) 76–84.
- [3] K. Hirao, T. Nagaoka, M.E. Brito, S. Kanzaki, *J. Am. Ceram. Soc.* 77 (7) (1994) 1857–1862.
- [4] E. Tani, S. Umebayashi, K. Kishi, K. Kobayashi, M. Nishijima, *Am. Ceram. Soc. Bull.* 65 (9) (1986) 1311–1315.
- [5] P.F. Becher, E.Y. Sun, K.P. Plucknett, K.B. Alexander, C.H. Hsueh, H.T. Lin, S.B. Waters, C.G. Westmoreland, *J. Am. Ceram. Soc.* 81 (11) (1998) 2821–2830.
- [6] Q. Wei, J. Sankar, J. Narayan, *Ceram. Eng. Sci. Proc.* 20 (3) (1999) 463–472.
- [7] M.M. Chadwick, D.S. Wilkinson, *J. Am. Ceram. Soc.* 75 (1992) 2327–2334.
- [8] J. Crampon, R. Duclos, N. Rakotoharisoa, *J. Mater. Sci.* 28 (1993) 909–916.
- [9] C.J. Gasdaska, *J. Am. Ceram. Soc.* 77 (1994) 2408–2418.
- [10] W.E. Luecke, S.M. Wiederhorn, B.J. Hockey, R.F. Krause, G.G. Long, *J. Am. Ceram. Soc.* 78 (1995) 2085–2096.
- [11] C.W. Li, F. Reidinger, *Acta Mater.* 45 (1997) 407–421.
- [12] R.F. Krause, Jr., W.E. Luecke, J.D. Frenck, B.J. Hockey, S.M. Wiederhorn, *J. Am. Ceram. Soc.* 82 (1999) 1233–1241.
- [13] W.E. Luecke, S.M. Wiederhorn, *J. Am. Ceram. Soc.* 82 (1999) 2769–2778.
- [14] K.C. Liu, C.O. Stevens, C.R. Brinkman, J.O. Kiggans, T.N. Tiegs, *Ceram. Eng. Sci. Proc.* 17 (3) (1996) 401–410.
- [15] J.J. Thomas, H.M. Jennings, D.L. Johnson, *MRS Symp. Proc.* 287 (1992) 277.
- [16] T.N. Tiegs, J.O. Kiggans, Jr., H.T. Lin, C.A. Willkens, *MRS Symp. Proc.* 347 (1994) 501.
- [17] Y.C. Kim, D.K. Kim, C.H. Kim, K. Bai, J.W. Jun, *Ceram. Eng. Sci. Proc.* 18 (1997) 505.

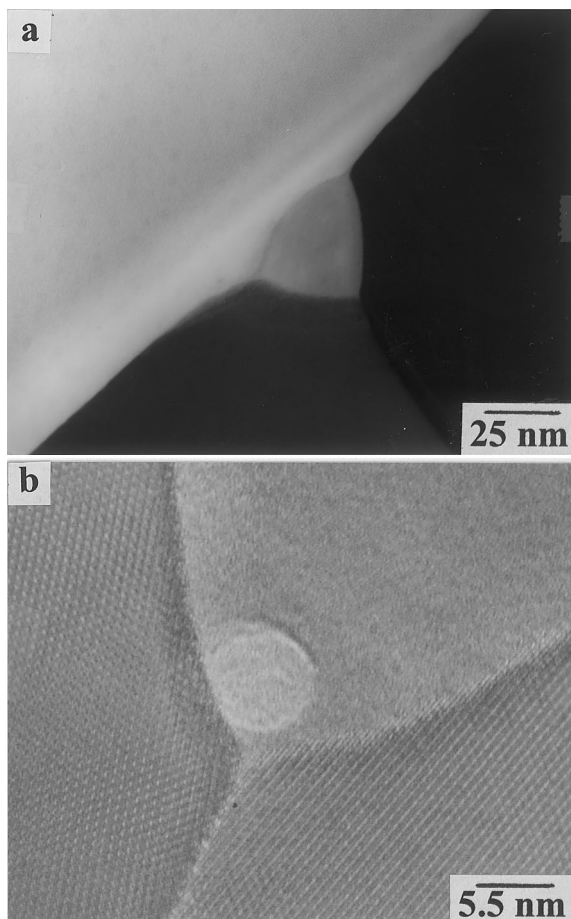


Fig. 10. TEM image of a typical triple junction phase in the microwave annealed GS44 (MA12-5) (a) and high-resolution lattice image of the β - Si_3N_4 grains and part of the triple junction phase. Lattice fringes are visible from the triple junction phase area.

- [18] V.P. Paranosenkov, Y.V. Bykov, V.V. Kholoptsev, A.A. Chikina, I.L. Shkarupa, A.V. Merkulova, Microwave Sintering of Silicon Nitride-Based Ceramics, *Ogneupory*, 1 Jan 1997 (in Russian).
- [19] Q. Wei, J. Sankar, A.D. Kelkar, J. Narayan, *Mater. Sci. Eng. A272* (1999) 380–388.
- [20] Q. Wei, J. Sankar, J. Narayan, A.D. Kelkar, *Proc. of 38th AIAA/SDM Conference, Part 2*, 983–991 (AIAA-97-1108) (1997).
- [21] M.K. Ferber, M.G. Jenkins, *J. Am. Ceram. Soc.* 75 (1992) 2455–2462.
- [22] M.K. Ferber, M.G. Jenkins, V.J. Tennery, *Ceram. Eng. Sci. Proc.* 11 (7–8) (1990) 1028–1037.
- [23] D.R. Clarke, *J. Am. Ceram. Soc.* 70 (1987) 15–22.